Quantification of global orbital shape variation

Alice Prevost, Samuel Muller, Frédéric Lauwers, Yann Heuzé

Received: 23 October 2022 | Revised: 22 December 2022 | Accepted: 24 December 2022

DOI: 10.1002/ca.24007

COMMUNICATION

CLINICAL ANATOMY WILEY

Quantification of global orbital shape variation

Alice Prevost[1] | Samuel Muller[2] | Frédéric Lauwers[1] | Yann Heuzé[3]

[1]Plastic and Maxillo-facial Surgery Department, University Hospital Center of Toulouse, Toulouse, France

[2]Plastic and Maxillo-facial Surgery Department, Ramsay Santé Clinique de l'Union, Toulouse, France

[3]Univ. Bordeaux, CNRS, MC, PACEA, Pessac, France

Correspondence
Alice Prevost, Plastic and Maxillo-facial Surgery Department, CHU Purpan, Place du Dr Baylac, F-31059 Toulouse Cedex, France.
Email: prevost.a@chu-toulouse.fr

Abstract

The complex anatomy of the orbit generates a complex orbital shape that can only be quantified approximatively by classic linear measurements such as maximum width and height. There is no global three-dimensional quantification of variations in orbital shape. The purpose of this study was to develop a method to quantify a global three-dimensional orbital shape variation in a healthy population and to test a series of explanatory factors. We investigated the hypotheses that orbital shape is related to gender(H1), orbital size(H2) and/or age(H3). Medical computed tomography(CT) images of 60 adult individuals were studied. The study sample consisted of 30 males and 30 females with a mean age of 25.1 years. Four anatomical landmarks and 140 semi-landmarks were measured on both positive and negative 3D reconstructed orbits and analyzed with geometric morphometrics. A principal component analysis(PCA) was computed to define a morphological space. Shape variation was visualized using vector distance maps and diagrams. The greatest variation was seen in the length of the superior orbital fissure. There was a gradient in terms of orbital shape ranging from short, wide orbits to tall, narrow orbits. The analysis did not highlight any significant age-, gender- or size-related impact in terms of orbital shape variation. Future avenues to explore include the study of other potential explanatory factors such as the different embryological origins of the orbital bones, the passage of vessels and nerves, and ethnic origins. This method can also be applied to the study of pathological orbits.

KEYWORDS
anatomic variation, anatomy, ophthalmological surgical procedure, orbit

1 | INTRODUCTION

It is challenging to study orbital shape because of its complex anatomy. However, it is pivotal for surgeons to quantify orbital shape as accurately as possible prior to access or repair (Farkas et al., 1972, 1989; Farkas & Deutsch, 1996). Quantification of morphological variation benefits from the advantages of imaging techniques. Computed tomography (CT) and, more recently, cone beam (CB) are now widely used in orbital measurements. These measurements are comprehensive and facilitate inter-population comparisons as well as the study of facial growth and aging (Buziashvili et al., 2019; Farkas et al., 2005; Paskhover et al., 2017; Weaver et al., 2010). The most common measurements of the orbit are height, width, depth, inter-orbital distance (Weaver et al., 2010) and orbital volume (Andrades et al., 2018; Kwon et al., 2010).

Classic morphometric studies highlight considerable variation in these measurements, which can be explained by intra- and inter-population variability (Feng et al., 2020; Kim et al., 2020; Moon

et al., 2020; Pessa et al., 1999). However, variation can also be explained to a significant extent by methodological differences in orbit measurements (Sentucq et al., 2020). Although the orbit is studied from a three-dimensional perspective, the vast majority of measurements are recorded in two dimensions, which does not facilitate comprehensive investigation of orbital conformation. Furthermore, despite extensive studies conducted with CT data, definition of the anterior limit of the orbit nevertheless remains challenging. (Osaki et al., 2013).

The accurate and reliable quantification of global orbital shape variation poses another challenge. Indeed, the orbit has a complex shape and a large number of linear measurements in the three spatial planes are required to properly quantify its morphological variation. Classic morphometry does not appear commensurate with an accurate, reliable, comprehensive and global quantification of 3D orbital shape variation. It is therefore critical to explore alternative methods and to investigate explanatory factors.

The purpose of this study was to develop a method using geometric morphometrics (Rohlf & Slice, 1990) to quantify 3D orbital shape variation and to test a series of explanatory factors. We investigated the hypotheses that orbital shape is related to gender (H1), orbit size (H2) and/or age (H3). We endeavored to locate and measure the extent of this variation over the entire orbital surface. This method was applied to a sample of the general population in order to study the characteristics of a healthy orbit.

2 | PATIENTS AND METHODS

2.1 | Study population

The patients enrolled in the study underwent scans in the Emergency Department of Toulouse Purpan University Hospital between April 2016 and April 2018. DICOM (Digital Imaging and Communications in Medicine) files were obtained from CT scans. These scans were performed due to suspected facial fractures or facial cellulitis. The number of subjects required to demonstrate sexual dimorphism could not be calculated a priori. We analyzed a population of 60 healthy patients divided into two groups of 30 patients according to gender.

To be enrolled in the study, patients had to be between 18 and 30 years of age and have had a CT scan of the facial mass with or without contrast medium (GE Medical System scanner, Optima CT660 model). This age limit was set to restrict measurement bias due to age-related changes in orbital shape (Ahmadi et al., 2007).

Patients with a history of craniofacial malformation, injury or tumor, or whose CT scan revealed craniofacial injury or tumor were excluded from the study.

The anonymised images were then exported in DICOM format in slices 0.6 mm thick.

Only the right orbit was analyzed for each patient as studies based on bilateral measurements of orbital dimensions and volume did not highlight any significant differences between the two orbits (Andrades et al., 2018; Ji et al., 2010). The local Institutional Review Board approved this study.

2.2 | Definition of landmarks

A three-dimensional mesh (.stl) representing the orbital content, i.e. the negative volume of the bony orbit, was used to study variations in orbital conformation [Stratovan Maxillo™ software (Strong et al., 2013)].

Geometric morphometry (GM) is based on the acquisition, processing and analysis of landmarks measured on objects, the morphological variation of which is to be quantified, regardless of variation related to position, orientation and scale (Rohlf & Slice, 1990). GM therefore characterizes the shape of the object by the set of landmark coordinates on the surface of the object (Strong et al., 2013).

Landmarks can be categorized in several ways but are broadly subdivided into "anatomical" landmarks and semi-landmarks (Bookstein, 1997). Anatomical landmarks (LM) are discrete anatomical loci that are biologically homologous. A semi-landmark (SL) refers to any point on a geometric element defined by its position on that element. Furthermore, Weber and Bookstein (Weber, 2015) defined three types of SL: SL on curves; SL on surfaces and constructed SL (i.e. at the beginning and end of a curve).

We have defined a set of four LMs and 140 SLs measured on each individual in our sample.

2.2.1 | Definition of the anatomical landmarks

For the orbital cone study, we defined four LMs: the anterior border of the superior orbital fissure, the anterior border of the inferior orbital fissure, the outer border of the lacrimal fossa and the inferior border of the optic canal (Figure 1).

The selection of LMs used in the present study was guided by earlier work (Khonsari et al., 2016; Rontal et al., 1979; Sarkar et al., 2021). The repeatability (i.e. intra-observer error test) of the measurements was assessed with the intraclass correlation coefficient (ICC, two-way mixed-effects model, perfect agreement) (Rosner, 2010) (Rosner, 2010). Ten right orbits were used to assess the repeatability of the measurements. One observer (AP) measured the landmarks on these 10 orbits three times on different days. The ICC ranged from 0.931 to 0.982 for the different measurements studied, thus indicating excellent reliability (Annex A).

2.2.2 | Definition of the semi-landmarks

We defined 120 surface SLs to characterize the surface of the orbital cone, and 20 curve SLs to characterize the orbital margin (and thus the anterior wall).

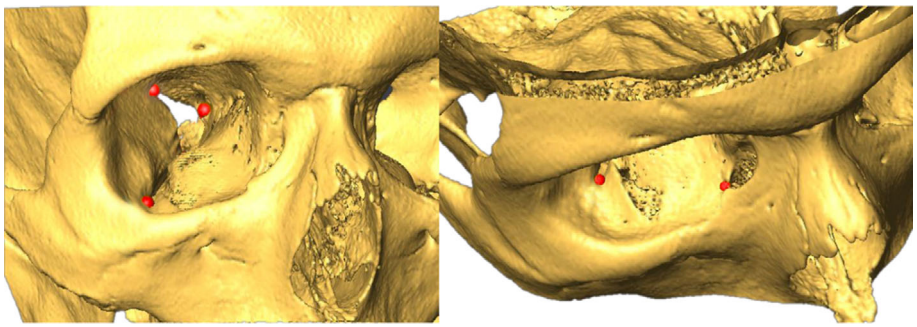

FIGURE 1 Positioning of the four anatomical landmarks on the 3D representation of the facial skeleton

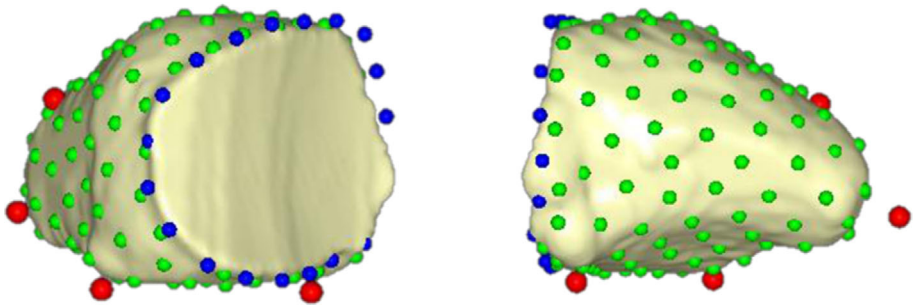

FIGURE 2 Landmarks: Anatomical landmarks (red), curved semi-landmarks (blue), and surface semi-landmarks (green) on the negative volume of the right orbit. Floating points (red and blue) were measured on the positive reconstruction of the orbit.

To ensure geometric homology between the corresponding SLs, we slid the SLs using an algorithm that minimizes bending energy ("thin-plate spline" algorithm) (Bookstein, 1997; Dunn, 1993) .

One hundred and forty-four LMs and SLs were thus positioned per object and distributed as follows: 120 surface SLs on the orbital cone, 20 curve SLs on the orbital margin contour and 4 LMs (Figure 2). The anatomical LMs and curve SLMs were positioned on the 3D orbital reconstructions, unlike the surface SLs which were placed on the negative volume of the orbit.

The coordinates of the 144 landmarks of each patient were exported for geometric morphometric analysis.

2.3 | Statistical evaluation of the variation in orbit shape

2.3.1 | Procrustes superimposition

We performed Procrustes superimposition (Goodall, 1991; Klingenberg, 2011; Rohlf & Slice, 1990) of the coordinates for the 144 LMs and SLs of the 60 study patients. This superimposition allows the geometric characteristics of the object to be studied separately in terms of scale, position and orientation in space (Rohlf & Slice, 1990). For each individual, we estimated the centroid size ("CS": square root of the sum of the squared distances of the landmarks to the centroid) and subsequently used CS as a proxy for orbital size. The average orbital shape was obtained by averaging the Procrustes coordinates of all the orbits. The quantitative variables recorded for each patient were age and orbital volume, expressed in cm3.

2.3.2 | Principal component analysis

To quantify orbital morphological variation, we produced a covariance matrix and then performed a principal component analysis (PCA) to reduce the dimensions of the dataset and explore individual positioning in the shape space. Only principal components (PC) representing more than 5% of the total variance were analyzed. "Lollipop" diagrams were used to investigate the variation in orbital shape for the PCs analyzed. This representation highlights the direction and extent of the variations through vectors. The vector starting point represents the landmark considered in the (virtual) average orbit. The end of the vector represents the position of the landmark considered in the orbit corresponding to the selected PC score.

For each PC, we then determined the coordinates of the LMs and SLs of the orbits occupying the shape space in the PC score range (positive and negative) and reconstructed the corresponding virtual orbits in 3D by deformation (TPS) to portray variations in orbital shape more clearly. These orbits were then compared by measuring vector distances, represented graphically by a three-dimensional vector distance map. This approach was used to visualize the 'range' of orbits in the male and female groups and to visually assess the differences in orbital conformations.

2.3.3 | Quantification of sexual dimorphism and assessment of the impact of age and size on orbital shape

We performed multiple multivariate regression analyses to assess the impact of age and orbital size (centroid size) on orbital shape. The

independent variables studied were age and centroid size versus orbital shape (dependent variable).

We then looked for sexual dimorphism by comparing the female average shape to the male average shape. The result was expressed as Procrustes distance (square root of the summed squared distance between homologous landmarks in two landmark configurations after Procrustes superimposition) (Kendall, 1984).

2.4 | Software used

We used Stratovan Maxillo™ software to create the STL file of the orbital volume (negative volume of the bony orbit). This software package was specifically developed to extract the orbital volume and shape from patients' CT scans. This information was then exported in a surface file (mesh.stl) format (Strong et al., 2013).

Avizo (Thermo Scientific™ Avizo™ software) was used to position the LMs on the 3D orbit reconstructions, and to reconstruct virtual 3D deformed orbits (TPS) from the coordinates of the LMs and SLs of the orbits associated with the range of PC scores in order to portray variation in orbital shape. These orbits were then compared by measuring vector distances, represented graphically by a three-dimensional vector distance map ("Vertex differences" function which calculates vector distances between homologous mesh vertices). The semi-automated procedure of measuring the SLs on the negative volume of the orbit using the TPS algorithm was performed with Viewbox software (dHAL, Athens, Greece).

The Procrustes superimposition and subsequent statistical analyses were performed with MorphoJ software (Klingenberg, 2011).

3 | RESULTS

3.1 | Analysis of the main morphological orbital variation

The study sample consisted of 30 males and 30 females with a mean age of 25.1 years. The female group was significantly older than the male group with an average age of 26.9 years versus 23.7 years, respectively (t test, $p = 0.003$).

3.1.1 | Orbital shape analysis

The PCA performed on the 60 individuals highlighted 5 PCs with over 5% percentage variance (Figure 3). The cumulative percentage of variance of these 5 PCs was 67% (Figure 3).

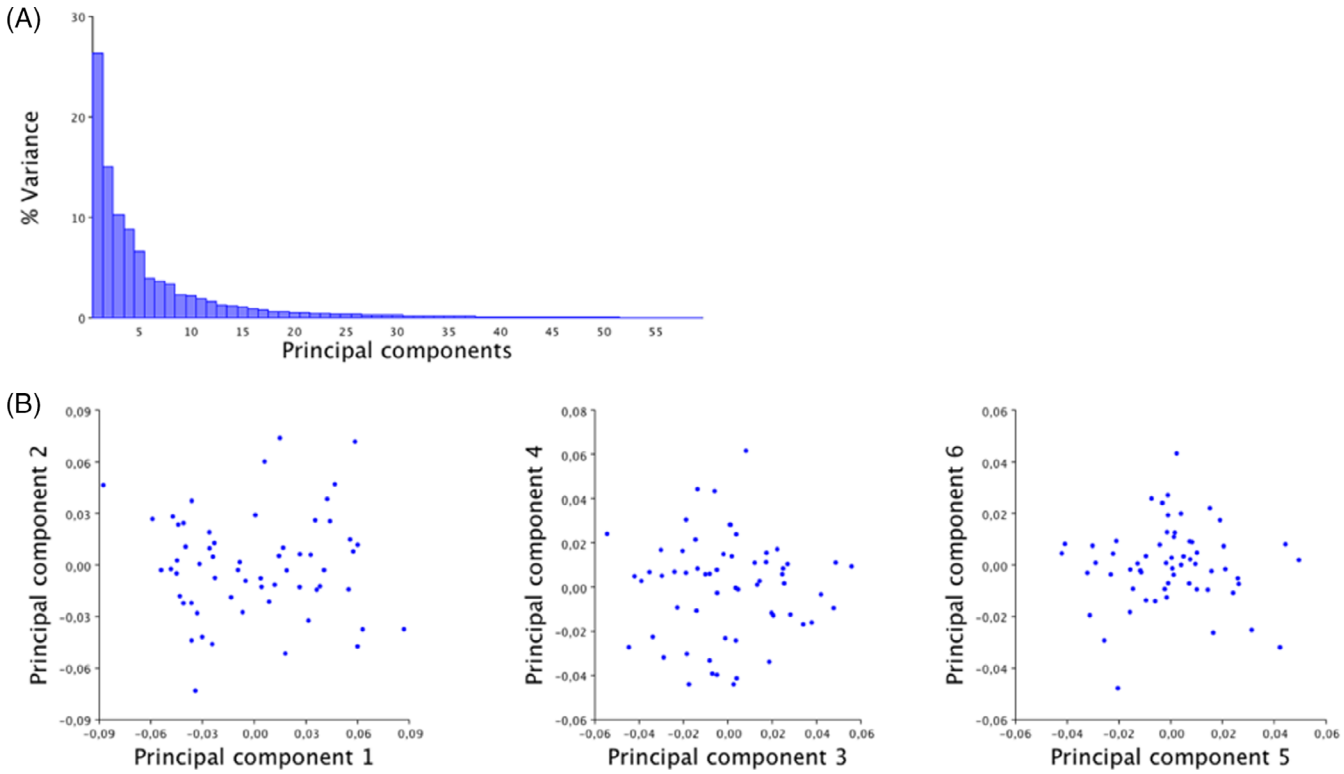

FIGURE 3 Graph highlighting PC distribution: (A) Histogram of variances. (B) Distribution of PCs. PC1 (% variance = 26.325%). Option to separate individuals into 2 groups, based on the values −0.03 and + 0.03, PC2 (% variance = 15.022%). Homogeneous distribution with a concentration of orbits around the mean value, PC3 (% variance = 10.284%). Homogeneous distribution with a concentration of orbits around the mean value, PC4 (% variance = 8.834%). High concentration of orbits around the mean value, PC5 (% variance = 6.632%). Low dispersion of orbits with the majority ranging from −0.03 to +0.03.

3.1.2 | Quantification of the morphological variations of the orbit

The main geometric variations are summarized in Table 1.

PC1 accounted for about 27% of the total variance. The orbital shape denoted by PC1 then represents over one-quarter of the orbit morphological variation of our 60 patients (Figure 3). Vector analysis shows that the main variations represented by PC1 reflect orbital height and length. As the height increases, the length decreases. The orbital aspects displaying the largest shape variation on PC1 were the posterior-superior region of the orbit and the superior orbital margin. The vector distance map analysis of PC1 showed these localized anatomical variations. The former region corresponded to the anterior extremity of the superior orbital fissure (Figure 4). PC1 highlighted the variation in the relative length of the superior orbital fissure.

PC2 and PC3 showed the global deformation of the orbit. A vector distance map analysis of PC2 (Supplementary data, Annex B) highlighted the stability of the roof of the orbit and considerable differences in the external and inferior orbital margins. The largest differences in relation to shape were found in the medial canthal region and inferolateral angle. A slight variation is apparent only in the upper portion of the orbit opposite the lacrimal fossa. All of these shape changes appear to be explained by a change in the angle of the orbital apex associated with a change in the length of the external wall. Analysis of the vector distance maps in PC3 showed that the orbital apex was the most variable region. Differences were also evident in the two orbital fissures. While a significant variation in the superior orbital fissure was highlighted in PC1, the variation in the inferior orbital fissure was evident only from PC3. Analysis of PC4 showed variations in the medial canthal region and the orbital apex, explained by elongation of the medial orbital wall. The main consequence is the change in direction of the anterior orbital wall. The main variations in PC5 were in the anterior portion of the roof of the orbit opposite the lacrimal fossa, and in the superior orbital fissure.

3.1.3 | Potential impact of gender, size, and age on orbital shape

The Procrustes distance between the average male and female orbits was 0.026 ($p = 0.07$). Therefore, no significant sexual dimorphism of the orbital region was evident in our sample. There was no significant difference in orbital shape between the male and female subjects in this study ($d = 0.026$; $p = 0.07$).

Comparison of orbital volumes and centroid size (Table 2) showed that male orbits were significantly larger than female orbits (Table 2).

Multiple multivariate regression of orbit shape (dependent variable) on centroid size (independent variable) was not significant ($R^2 = 0.0165$; $p = 0.42$). Therefore, orbit size did not significantly impact orbit shape. In other words, there was no significant allometry in orbit shape. There was no significant correlation between the first five PCs and the centroid size of the orbit (Table 3).

The potential impact of age on orbit shape was investigated separately for males and females given the significant difference in mean age between the male and female subjects. A significant age-related impact on orbit shape was not apparent in either the males or the females, as confirmed by non-significant multivariate multiple regressions ($R^2 = 0.0272$; $p = 0.63$ for males and $R^2 = 0.0174$; $p = 0.93$ for females).

TABLE 1 Summary of main orbital variations depending on PC

	Variance %	Variations observed
PC1	27	Relative length of the superior orbital fissure
PC2	14.2	Anterior posterior and transverse dimensions Inferior orbital margin, Medial/lateral canthal regions
PC3	10.4	Anterior posterior dimension Inferior orbital fissure Superior orbital fissure
PC4	9	Medial wall length
PC5	6.8	Lacrimal fossa region Superior orbital fissure

4 | DISCUSSION

4.1 | Main morphological variation and explanatory factors

The main outcome of the present study involving a healthy cohort is the identification of two patterns of orbit shape variation within the general population. There are one-off changes in a specific orbital region, such as those observed in PC1, PC4 and PC5, and global changes in orbit shape, as in PC2 and PC3 relating to an opening in the angle of the orbital apex.

When gender was used as a classifier with the PCA of the Procrustes shape coordinates, no obvious data separation was noted. Similarly, there were no significant differences in shape between the average male and average female orbit. Hypothesis H1 is therefore not corroborated by our data. Our results also show that orbit shape is not significantly correlated with orbit size or age, thus refuting H2 and H3, respectively.

The main axis of variation (PC1) showed strong individual variation in the length of the superior orbital fissure, highlighting this aspect of the orbit as the main site of inter-individual variation in a healthy population. This fissure is bound by the greater and lesser wings of the sphenoid. It provides a thoroughfare for vascular and neural structures to enter the orbit. It is widely noted that anatomy is function-dependent. The size of the orbital fissure is therefore probably associated with the volume of structures passing through it (Moss & Salentijn, 1969). Future work will focus on this hypothesis by measuring those structures and testing for correlation with fissure length.

Furthermore, the size of this fissure most certainly depends on the respective growth of the greater wing and lesser wing of the sphenoid. A recent study (Yamamoto et al., 2021) showed that the greater wing of the sphenoid derives from endochondral bones (i.e. ala temporalis and alar process) and multiple membranous bones,

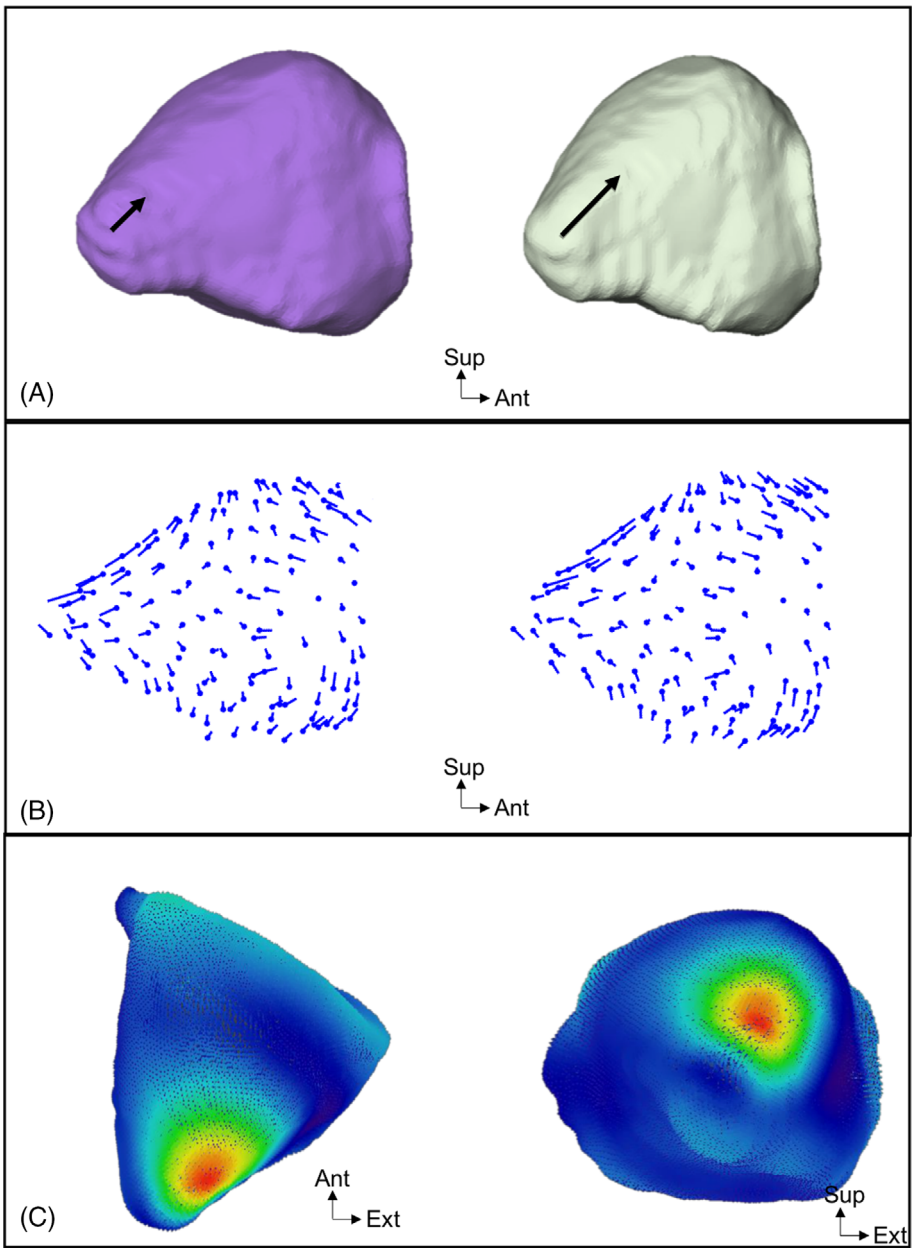

FIGURE 4 Different graphical representations of the variations in configurations present on PC1: (A) Three-dimensional representation of the orbital volume, posterior view. The length of the superior orbital fissure is depicted with an arrow (green: +0.06; purple: −0.06). (B) Lollipop representation (scale factor = −0.06 to the left, +0.06 to the right). (C) Vector distance map comparing the orbits on PC1, superior view to the left and posterior view to the right.

TABLE 2 Comparison of orbital volumes and centroid sizes

	Women $n = 30$	Men $n = 30$	p
Orbital volume (cm^3)	27.3	30.4	$p < 0.0001$
Centroid size	241.5	247.7	$p < 0.001$

TABLE 3 Effect of centroid size on each PC. p(permutation test 10,000)

PC	% Predicted	p
PC1	0.03%	0.87
PC2	1.56%	0.33
PC3	0.15%	0.76
PC4	5.96%	0.06
PC5	1.78%	0.30

whereas the lesser wing derives from a single cartilaginous structure (the orbitosphenoid). Assuming that the ossification of the greater wing of the sphenoid is membranous in origin while the lesser wing is cartilaginous, their growth patterns are likely to be differential.

The secondary shape variation axis (PC2) showed more global deformation in the orbit with only the orbit roof displaying some inter-individual stability. This change in shape impacts the three dimensions of the orbit. It is interesting to note that this deformation is indicative of the orbital index (Piquet, 1954). The latter is expressed

as the centesimal height to width ratio of the orbital frame [(orbital height x100)/orbital width]. Thus, orbits corresponding to minimum values on PC2 would have a high orbital index, while orbits with positive values on PC2 would have a low orbital index.

Anthropological studies agree that it is impossible to determine the gender of an individual by the shape of the orbit (Husmann & Samson, 2011), as corroborated by our results.

4.2 | Originality of the study

Geometric morphometrics is a method widely used in statistical shape analysis, particularly in evolutionary biology. This method is specifically designed to conduct quantitative analyses of shape variation regardless of position, orientation and scale. Geometric morphometrics is far less common in the medical field. For the face and its skeleton, this method is used to adapt cephalometric studies to 3D (Olszewski et al., 2010). Some studies focus on sexual dimorphism features in the craniofacial skeleton (Bigoni et al., 2010; Gonzalez et al., 2011; Koudelová et al., 2015). This is the first time that the global morphological variation of the orbit has been quantified using this method.

In addition, our methodology can be used to characterize the limitation of the anterior orbital wall, thereby complementing previously published morphometry protocols (Nilsson et al., 2018).

Our study is the first to report on the absence of a statistically significant correlation between orbital shape and gender, age and orbital volume.

4.3 | Study limitations

The age limit imposed by our inclusion criteria was set to prevent measurement bias linked to changes in orbital shape with age. Indeed, current studies measuring orbital dimensions as a function of age identify an increase in orbital size up to 18 to 20 years of age. New orbital frame deformities (increase in the width and area of the orbital aperture, and modification of the orbital rim), appear after the age of 30 (Kahn & Shaw, 2008; Richard et al., 2009; Weaver et al., 2010). The regression analysis performed confirms that age is not a confounding factor in our study.

As CT images were obtained retrospectively and anonymously (only age and gender were reported), the ethnic or geographical origin of the individuals could not be taken into account although inter-ethnic orbital variation has been demonstrated with differences highlighted in the shape of the orbital contour (Xing et al., 2013) as well as in inter-pupillary distances and the width of the palpebral fissure (Barretto & Mathog, 1999).

Our analysis is based on 3D coordinates of anatomical points and points semi-automatically positioned on the surface of the orbit. The choice of the anatomical points is crucial for reliable measurements. The decisive criterion is the repeatability and reproducibility of the positioning of these points and their consistency. Studies using intra-orbital anatomical LMs are very sparse. The four anatomical LMs we selected are those used in recent three-dimensional orbital morphometric studies (Dunn, 1993; Khonsari et al., 2016). They are well delineated, repeatable and reproducible. It is not surprising to find variation at the medial canthal level for each of the PCs. Indeed, this is a diffuse anatomical region which, along with orbital fissures, is difficult to delineate using Stratovan Maxillo software. However, the variation in relative length shown on PC1 is mostly due to the position of the LM placed at the end of the superior orbital fissure. The latter was manually positioned on a high-definition scanner and chosen specifically for its reproducibility. Therefore, this is a reliable LM that ensures the quality of the analysis of the length of the superior orbital fissure.

When investigating the impact of orbit size on its morphology (H2), it seemed more relevant to us to use centroid size as an independent variable rather than orbital volume. Indeed, centroid size is based on the surface SLs as well as on the LMs and curve SLs positioned on the three-dimensional reconstructions. As stated above and as shown in Figure 2, Stratovan Maxillo software has some inaccuracies regarding the orbital and medial cantal apex. Consequently, the negative volume computed by Stratovan might be less reliable than the centroid size.

4.4 | Perspectives and conclusions

This pilot study proposes methodology to quantify the variation in global orbit shape and locate the main variation sites in order to gain a better understanding of the mechanisms and pathophysiology of certain deformities.

One perspective arising from this work will be to further explore the relationship between the size of the vessels/nerves and the orbit shape. Indeed, we suggest that the difference noted in superior orbital fissure morphology is linked to the volume of the structures which cross it and/or to the differential growth of the lesser and greater wings of the sphenoid.

The second perspective will be the study of orbital allometry during growth, i.e. the differential growth of the various bones involved. The orbit comprises seven different bones of various embryological origins. While the development of each of the facial and neurocranial bones can be seen individually, it is far more difficult to get an integrative approach of the growth of the entire orbit. It should be possible to pinpoint the sites of age-related variation using geometric morphometrics to study the orbit ontogenetic trajectory. It is challenging to statistically compare an adult orbit to that of a child as all of the dimensions of the latter will differ due to the considerable size difference. By overcoming the scale effect and allowing the allometric component of shape variation to be quantified, Procrustes superimposition allows changes in orbit shape to be compared during growth and, at the same time, to the adult orbit shape. The location and extent of orbital changes during various growth periods could be determined. The growth trajectory of the different orbital regions could then be established by correlating changes in shape to the anatomy.

The third perspective will be to focus on the impact on orbit morphology of late maturation from 20 to 80 years of age.

Last but not least, the methodology used in the present study could enhance our knowledge of the pathological orbit. Indeed, by creating the average orbit of a syndrome associated with orbital dysmorphology, it will be possible (by comparing it with the average orbit of a population of the same gender and age) to highlight those regions affected in order to characterize and gain a better understanding of these dysmorphologies.

FUNDING INFORMATION

None.

ORCID

Alice Prevost https://orcid.org/0000-0003-2903-0644

REFERENCES

Ahmadi, H., Shams, P. N., Davies, N. P., Joshi, N., & Kelly, M. H. (2007). Age-related changes in the normal sagittal relationship between globe and orbit. *Journal of Plastic Reconstructive and Aesthetic Surgery*, *60*, 246–250.

Andrades, P., Cuevas, P., Hernández, R., Danilla, S., & Villalobos, R. (2018). Characterization of the orbital volume in normal population. *Journal of Cranio-Maxillo-Facial Surgery*, *46*, 594–599.

Barretto, R. L., & Mathog, R. H. (1999). Orbital measurement in black and white populations. *Laryngoscope*, *109*, 1051–1054.

Bigoni, L., Velemínská, J., & Brůžek, J. (2010). Three-dimensional geometric morphometric analysis of cranio-facial sexual dimorphism in a central European sample of known sex. *Homo – Journal of Comparative Human Biology*, *61*, 16–32.

Bookstein, F. L. (1997). Morphometric tools for landmark data: geometry and biology.

Buziashvili, D., Tower, J. I., Sangal, N. R., Shah, A. M., & Paskhover, B. (2019). Long-term patterns of age-related facial bone loss in black individuals. *JAMA Facial Plastic Surgery*, *21*, 292–297.

Dunn, G. (1993). Morphometric tools for landmark data: Geometry and biology. *Statistics in Medicine*, *12*, 714–715.

Farkas, L. G., & Deutsch, C. K. (1996). Anthropometric determination of craniofacial morphology. *American Journal of Medical Genetics*, *65*, 1–4.

Farkas, L. G., Katic, M. J., Forrest, C. R., Alt, K. W., Bagic, I., Baltadjiev, G., Cunha, E., Cvicelová, M., Davies, S., Erasmus, I., Gillett-Netting, R., Hajnis, K., Kemkes-Grottenthaler, A., Khomyakova, I., Kumi, A., Kgamphe, J. S., Kayo-daigo, N., Ie, T., Malinowski, A., … Yahia, E. (2005). International anthropometric study of facial morphology in various ethnic groups/races. *The Journal of Craniofacial Surgery*, *16*, 615–646.

Farkas, L. G., Lindsay, W. K., & Vanderby, M. B. (1972). Morphology of the orbital region in adults following the cleft lip/palate repair in childhood. *American Journal of Physical Anthropology*, *37*, 65–73.

Farkas, L. G., Ross, R. B., Posnick, J. C., & Indech, G. D. (1989). Orbital measurements in 63 hyperteloric patients differences between the anthropometric and cephalometric findings. *Journal of Cranio-Maxillo-Facial Surgery*, *17*, 249–254.

Feng, W.-J., Li, F.-W., Zhan, W.-F., Lin, F.-C., & Luo, S.-K. (2020). Three-dimensional analysis of age-related orbital and Midfacial bone remodeling in Asians. *Dermatologic Surgery*, *46*, e139–e145.

Gonzalez, P. N., Bernal, V., & Perez, S. I. (2011). Analysis of sexual dimorphism of craniofacial traits using geometric morphometric techniques. *International Journal of Osteoarchaeology*, *21*, 82–91.

Goodall, C. (1991). Procrustes methods in the statistical analysis of shape. *Journal of the Royal Statistical Society: Series BM*, *53*, 285–321.

Husmann, P. R., & Samson, D. R. (2011). In the eye of the beholder: Sex and race estimation using the human orbital aperture*. *Journal of Forensic Sciences*, *56*, 1424–1429.

Ji, Y., Qian, Z., Dong, Y., Zhou, H., & Fan, X. (2010). Quantitative morphometry of the orbit in Chinese adults based on a three-dimensional reconstruction method. *Journal of Anatomy*, *217*, 501–506.

Kahn, D. M., & Shaw, R. B. (2008). Aging of the bony orbit: A three-dimensional computed tomographic study. *Aesthetic Surgery Journal*, *28*, 258–264.

Kendall, D. G. (1984). Shape manifolds, procrustean metrics, and complex projective spaces. *B London Mathematical Society*, *16*, 81–121.

Khonsari, R. H., Way, B., Nysjö, J., Odri, G. A., Olszewski, R., Evans, R. D., Dunaway, D. J., Nyström, I., & Britto, J. A. (2016). Fronto-facial advancement and bipartition in Crouzon–Pfeiffer and Apert syndromes: Impact of fronto-facial surgery upon orbital and airway parameters in FGFR2 syndromes. *Journal of Cranio-Maxillo-Facial Surgery*, *44*, 1567–1575.

Kim, M. J., Lee, M. J., Jeong, W. S., Hong, H., & Choi, J. W. (2020). Three-dimensional computer modeling of standard orbital mean shape in Asians. *Journal of Plastic Reconstructive and Aesthetic Surgery*, *73*, 548–555.

KLINGENBERG, C. P. (2011). MorphoJ: An integrated software package for geometric morphometrics. *Molecular Ecology Resources*, *11*, 353–357.

Koudelová, J., Brůžek, J., Cagáňová, V., Krajíček, V., & Velemínská, J. (2015). Development of facial sexual dimorphism in children aged between 12 and 15 years: A three-dimensional longitudinal study. *Orthodontics and Craniofacial Research*, *18*, 175–184.

Kwon, J., Barrera, J. E., & Most, S. P. (2010). Comparative computation of orbital volume from axial and coronal CT using three-dimensional image analysis. *Ophthalmic Plastic Reconstructive Surgery*, *26*, 26–29.

Moon, S. J., Lee, W. J., Roh, T. S., & Baek, W. (2020). Sex-related and racial variations in orbital floor anatomy. *Archives of Craniofacial Surgery*, *21*, 219–224.

Moss, M. L., & Salentijn, L. (1969). The primary role of functional matrices in facial growth. *American Journal of Orthodontics*, *55*, 566–577.

Nilsson, J., Nysjö, J., Carlsson, A.-P., & Thor, A. (2018). Comparison analysis of orbital shape and volume in unilateral fractured orbits. *Journal of Cranio-Maxillo-Facial Surgery*, *46*, 381–387.

Olszewski, R., Tanesy, O., Cosnard, G., Zech, F., & Reychler, H. (2010). Reproducibility of osseous landmarks used for computed tomography based three-dimensional cephalometric analyses. *Journal of Cranio-Maxillo-Facial Surgery*, *38*, 214–221.

Osaki, T. H., de Castro, D. K., Yabumoto, C., Mingkwansook, V., Ting, E., Nallasamy, N., Curtin, H., & Fay, A. (2013). Comparison of methodologies in volumetric Orbitometry. *Ophthalmic Plastic and Reconstructive Surgery*, *29*, 431–436.

Paskhover, B., Durand, D., Kamen, E., & Gordon, N. A. (2017). Patterns of change in facial skeletal aging. *JAMA Facial Plastic Surgery*, *19*, 413–417.

Pessa, J. E., Desvigne, L. D., Lambros, V. S., Nimerick, J., Sugunan, B., & Zadoo, V. P. (1999). Changes in ocular globe-to-orbital rim position with age: Implications for aesthetic blepharoplasty of the lower eyelids. *Aesthetic Plastic Surgery*, *23*, 337–342.

Piquet, M.-M. (1954). L'indice orbitaire et l'appréciation de la largeur de l'orbite ; essai de standardisation. *Bulletins et Mémoires de la Société d'Anthropologie de Paris*, *5*, 100–112.

Richard, M. J., Morris, C., Deen, B. F., Gray, L., & Woodward, J. A. (2009). Analysis of the anatomic changes of the aging facial skeleton using computer-assisted tomography. *Ophthalmic Plastic and Reconstructive Surgery*, *25*, 382–386.

Rohlf, F. J., & Slice, D. (1990). Extensions of the Procrustes method for the optimal superimposition of landmarks. *Systematic Zoology*, *39*, 40.

Rontal, E., Rontal, M., & Guilford, F. T. (1979). Surgical anatomy of the orbit. *Annals of Otology, Rhinology and Laryngology*, *88*, 382–386.

Rosner, B. (2010). *Fundamentals of biostatistics* (7th ed., p. 303). Éd.

Sarkar, S., Baliga, M., Prince, J., Ongole, R., & Natarajan, S. (2021). Morphometric and volumetric measurements of orbit with cone-beam

computed tomography. *Journal of Oral and Maxillofacial Surgery*, *79*, 652–664.

Sentucq, C., Schlund, M., Bouet, B., Garms, M., Ferri, J., Jacques, T., & Nicot, R. (2020). Overview of tools for measurement of the orbital volume and their applications to orbital surgery. *Journal of Plastic Reconstructive and Aesthetic Surgery*, *74*, 581–591.

Strong, E. B., Fuller, S. C., & Chahal, H. S. (2013). Computer-aided analysis of orbital volume. *Ophthalmic Plastic and Reconstructive Surgery*, *29*, 1–5.

Weaver, A. A., Loftis, K. L., Tan, J. C., Duma, S. M., & Stitzel, J. D. (2010). CT based three-dimensional measurement of orbit and eye anthropometry. *Investigative Ophthalmology and Visual Science*, *51*, 4892–4897.

Weber, G. W. (2015). Virtual anthropology. *American Journal of Physical Anthropology*, *156*, 22–42.

XING, S., GIBBON, V., CLARKE, R., & LIU, W. (2013). Geometric morphometric analyses of orbit shape in Asian, African, and European human populations. *Anthropological Science*, *121*, 1–11.

Yamamoto, M., Jin, Z., Hayashi, S., Rodríguez-Vázquez, J. F., Murakami, G., & Abe, S. (2021). Association between the developing sphenoid and adult morphology: A study using sagittal sections of the skull base from human embryos and fetuses. *Journal of Anatomy*, *239*, 1300–1317.

SUPPORTING INFORMATION

Additional supporting information can be found online in the Supporting Information section at the end of this article.

How to cite this article: Prevost, A., Muller, S., Lauwers, F., & Heuzé, Y. (2023). Quantification of global orbital shape variation. *Clinical Anatomy*, *36*(8), 1066–1074. https://doi.org/10.1002/ca.24007